INTERNATIONAL JOURNAL OF CLIMATOLOGY
Int. J. Climatol. **33**: 1936–1947 (2013)
Published online 13 July 2012 in Wiley Online Library
(wileyonlinelibrary.com) DOI: 10.1002/joc.3562

RMetS
Royal Meteorological Society

Temporal–spatial distribution of the predictability limit of monthly sea surface temperature in the global oceans

Jianping Li* and Ruiqiang Ding

State Key Laboratory of Numerical Modeling for Atmospheric Sciences and Geophysical Fluid Dynamics (LASG), Institute of Atmospheric Physics, Chinese Academy of Sciences, Beijing 100029, China

ABSTRACT: To examine atmospheric and oceanic predictability based on nonlinear error growth dynamics, the authors introduced recently a new method using the nonlinear local Lyapunov exponent (NLLE). In this study, the NLLE method is employed to investigate the temporal–spatial distribution of the limit of sea surface temperature (SST) predictability, based on reanalysis monthly SST data. The results show that the annual mean limit of SST predictability is the greatest in the tropical central–eastern Pacific (>8 months). Relatively high values were also obtained for the tropical Indian and Atlantic Oceans (5–8 months). In the northern and southern mid-high latitude oceans, the limit of SST predictability is less than 6 months, with a minimum value of only 2–3 months. The limit of SST predictability in different oceanic regions shows significant seasonal variations, related to the persistence barriers that occur during particular seasons. In addition to the well-known spring persistence barrier (SPB) in the tropical central–eastern Pacific, persistence barriers also occur in other ocean areas during seasons other than spring. A winter persistence barrier (WPB) exists in the southeastern tropical Indian Ocean and the northern tropical Atlantic. In the North Pacific and North Atlantic, a persistence barrier exists around July–September. These seasonal persistence barriers cause a relatively low limit of SST predictability when predictions are made across the season in which the barriers occur. In contrast, when predictions are made initiated from the season with a persistence barrier, the SST errors show rapid initial growth but slow growth in the following seasons, resulting in a relatively high limit in predictability. Analyses also indicate that the possibility of really eliminating the effects of persistence barriers on SST errors by improving ocean–atmosphere coupled general circulation models (CGCMs) or the data assimilation procedure is very low. Copyright © 2012 Royal Meteorological Society

KEY WORDS sea surface temperature; nonlinear local Lyapunov exponent; predictability; persistence barrier

Received 13 September 2011; Revised 8 June 2012; Accepted 23 June 2012

1. Introduction

Sea surface temperature (SST), which is one of the most important variables related to the global ocean–atmosphere system, is widely applied as a boundary condition for monthly to seasonal climate predictions (Palmer and Anderson, 1994; Chowdary *et al*., 2010, 2011). The importance of SST to accurate seasonal forecasting of extreme climate events has been increasingly recognized in recent decades (Goswami and Shukla, 1991; Bengtsson *et al*., 1993; Trenberth *et al*., 1998; Peng *et al*., 2000; Frederiksen *et al*., 2001; Kang and Shukla, 2006). To date, significant progress in SST prediction has been achieved using ocean–atmosphere coupled general circulation models (CGCMs) with various complexities (Chen *et al*., 1995; Barnston *et al*., 1999; Kug *et al*., 2007). However, SST in the current CGCMs can only be accurately predicted for limited lead times, thereby indicating that SST predictability is inherently limited. The limited predictability of SST may arise from incomplete or inaccurate observations in the initial ocean–atmosphere state or from the use of imperfect models (Collins *et al*., 2002). It is important to determine the limit of SST predictability, as such information could be used as a basic guideline in future improvements to forecasting models. The occurrence of spatial variations in the ocean–atmosphere coupling dynamics means that the limit of SST predictability may differ in different ocean areas. It is therefore an important task to investigate the temporal–spatial distribution of the limit of SST predictability.

The El Niño-Southern Oscillation (ENSO) phenomenon, which originates in the tropical Pacific, has a widespread effect on the global climate system; consequently, considerable research effort has been devoted to determining the limit of ENSO predictability. The limit of ENSO predictability is found to be model-dependent, ranging from a few months to several years (Philander, 1990; Latif *et al*., 1998; Collins *et al*., 2002; Jin *et al*., 2008; Luo *et al*., 2008; Stockdale *et al*., 2011). However, most ENSO forecast models suffer from a decrease in forecast skill during the boreal spring (March–May), which is known as the spring persistence barrier (SPB) (Webster and Yang, 1992). The accurate forecasting of

*Correspondence to: Dr J. Li, State Key Laboratory of Numerical Modeling for Atmospheric Sciences and Geophysical Fluid Dynamics (LASG), Institute of Atmospheric Physics, Chinese Academy of Sciences, P.O. Box 9804, Beijing 100029, China.
E-mail: ljp@lasg.iap.ac.cn

ENSO by more than a season or two in advance is apparently limited by the SPB phenomenon. Compared with ENSO, SST variability in the tropical Atlantic and Indian oceans is typically weaker, and is generally given little attention in global seasonal forecast systems. Yet SST variability in the tropical Atlantic and Indian oceans is by no means negligible and could have a substantial impact on the atmosphere and on seasonal weather patterns (Folland *et al*., 1986; Guan and Yamagata, 2003; Taschetto and Wainer, 2008; Ding *et al*., 2010a; Li *et al*., 2010; Li *et al*., 2011). Many recent research efforts are directed towards investigating the SST predictability in the tropical Atlantic and Indian oceans using statistical or dynamical models, revealing that the SST anomaly (SSTA) in these oceans can be well predicted up to one or two seasons in advance (Repelli and Nobre, 2004; Wajsowicz, 2005; Stockdale *et al*., 2006; Luo *et al*., 2007). In addition to the tropical SSTs, previous studies have demonstrated a connection between SSTA in mid-latitudes and anomalous atmospheric circulations in overlying and downstream regions (Davis, 1978; Namias, 1986; Wu and Liu, 2004; Frankignoul and Sennéchael, 2007; Zhao and Li, 2010; Wu *et al*., 2009, 2011; Nnamchi and Li, 2011; Nnamchi *et al*., 2011). Therefore, there exists a need to predict extratropical SSTs in advance, yet most previous studies have focused on tropical SSTs. As a result, little is known of the limit of SST predictability in the extratropical oceans.

The objective of this study is to determine the spatial distribution of the limit of SST predictability in the global oceans based on reanalysis SST data, which contain a large proportion of the real information regarding SST, including its variability and regional features of ocean–atmosphere coupling dynamics (Smith and Reynolds, 2004). Previous studies have investigated the prediction skill of global SST based on numerical models (Luo *et al*., 2005; Kug *et al*., 2007). However, almost all of numerical models in use today are imperfect and deficiencies remain in simulating SST variability (see online at http://iri.columbia.edu/climate/ENSO/currentinfo/archive). Model errors have a strong influence on estimates of SST predictability, meaning that such estimates are commonly model-dependent. Moreover, these studies provided only qualitative estimates of SST predictability, such as information on regions with either higher or lower skill but no quantitative estimate of the limit of SST predictability.

Given the lack of realistic CGCMs in predicting SST, it is more appropriate to determine its predictability limit based on reanalysis SST data. A new method to this problem, employing the nonlinear local Lyapunov exponent (NLLE), was recently introduced to investigate atmospheric and oceanic predictability (Chen *et al*., 2006; Li *et al*., 2006; Ding and Li, 2007; Li and Wang, 2008; Li and Ding, 2011). The NLLE measures the average growth rate of initial errors of nonlinear dynamical models without linearizing the governing equations. Using the NLLE and its derivatives, the limit of dynamical predictability of chaotic systems can be quantitatively determined. Compared to traditional Lyapunov exponents based on linear error dynamics, the NLLE is more suitable for determining quantitatively the predictability limit of a chaotic system (Astudillo *et al*., 2010; Rogberg *et al*., 2010). To apply the NLLE method to the study of atmospheric and oceanic predictability, a reasonable and efficient algorithm has been devised to enable estimates of the NLLE and its derivatives based on observational or reanalysis data (Ding *et al*., 2008; Li and Ding, 2011). Accordingly, the limit of SST predictability at each grid point over the global ocean can now be assessed using the NLLE method.

The reminder of this paper is arranged as follows. Section 2 describes the data used in this study. Section 3 introduces the NLLE method. Section 4 discusses the spatial distribution of the annual mean predictability limit of global SST. Section 5 presents spatial variations in the seasonal mean predictability limit of global SST. Finally, Section 6 provides a summary and concluding remark.

2. Data

The SST dataset used in this study is version 2 of monthly NOAA Extended Reconstructed SST (ERSST.v2) data on a $2^\circ \times 2^\circ$ spatial grid for the period 1854–2005 (Smith and Reynolds, 2004). The SST data used for ERSST.v2 are derived from the latest version of the Comprehensive Ocean–Atmosphere Data Set. ERSST.v2 has been proved to be reliable for climate analysis and modeling (Smith and Reynolds, 2004). Before applying the NLLE method, the annual cycle of SST data is first removed to obtain the SSTA. On the basis of the time series of SSTA, the limit of monthly SST predictability at each grid point can be determined by employing the NLLE method. The spatial distribution of the limit of SST predictability is then investigated. It should be noted that the time series of SST data extends from 1854 to 2005, meaning that it may contain variability on all time scales up to and including multi-decadal. It also possibly contains a secular trend associated with global warming (Lau and Weng, 1999). However, any multi-decadal variability or secular trend contained in SST data would have little effect on estimates of the predictability limit of monthly SST because the limit is generally less than 1 year. Thus, in the NLLE method, the raw time series of SSTA is directly used without processing.

3. Nonlinear local Lyapunov exponent (NLLE)

3.1. NLLE of an n-dimensional dynamical system

Consider a general n-dimensional nonlinear dynamical system whose evolution is governed by

$$\frac{d\mathbf{x}}{dt} = \mathbf{F}(x) \tag{1}$$

where $\mathbf{x} = [x_1(t), x_2(t), \cdots\cdots, x_n(t)]^{\mathrm{T}}$ is the state vector at the time t, the superscript T is the transpose, and $\mathbf{F}$

represents the dynamics. The evolution of a small error $\delta = [\delta_1(t), \delta_2(t), \cdots\cdots, \delta_n(t)]^{\mathrm{T}}$, superimposed on a state $\mathbf{x}$, is governed by the nonlinear equations:

$$\frac{d}{dt}\boldsymbol{\delta} = \mathbf{J}(\mathbf{x})\boldsymbol{\delta} + \mathbf{G}(\mathbf{x}, \boldsymbol{\delta}) \tag{2}$$

where $\mathbf{J}(\mathbf{x})\boldsymbol{\delta}$ are the tangent linear terms, and $\mathbf{G}(\mathbf{x}, \boldsymbol{\delta})$ are the high-order nonlinear terms of the error δ. Because of some difficulties in solving the nonlinear problem, most previous studies (Lorenz, 1965; Eckmann and Ruelle, 1985; Yoden and Nomura, 1993; Kazantsev, 1999; Ziehmann *et al*., 2000) assumed that the initial perturbations were sufficiently small that their evolution could be approximately governed by the tangent linear model of the nonlinear model. However, the tangent linear approximation to error growth equations is not applicable to situations in which the initial errors are not very small (Lacarra and Talagrand, 1988; Mu, 2000; Ding and Li, 2007; Li and Ding, 2011). Therefore, the nonlinear behaviors of error growth should be considered in determining the limit of predictability. Without a linear approximation, the solutions of Equation (2) can be obtained by numerically integrating it along the reference solution $\mathbf{x}$ from $t = t_0$ to $t_0 + \tau$:

$$\boldsymbol{\delta}_1 = \boldsymbol{\eta}(\mathbf{x}_0, \boldsymbol{\delta}_0, \tau)\boldsymbol{\delta}_0 \tag{3}$$

where $\boldsymbol{\delta}_1 = \boldsymbol{\delta}(t_0 + \tau)$, $\mathbf{x}_0 = \mathbf{x}(t_0)$, $\boldsymbol{\delta}_0 = \boldsymbol{\delta}(t_0)$, and $\boldsymbol{\eta}(\mathbf{x}_0, \boldsymbol{\delta}_0, \tau)$ is the nonlinear propagator. The NLLE is then defined as

$$\lambda(\mathbf{x}_0, \boldsymbol{\delta}_0, \tau) = \frac{1}{\tau}\ln\frac{||\boldsymbol{\delta}_1||}{||\boldsymbol{\delta}_0||} \tag{4}$$

where $\lambda(\mathbf{x}_0, \boldsymbol{\delta}_0, \tau)$ depends in general on the initial state $\mathbf{x}_0$ in phase space, the initial error $\boldsymbol{\delta}_0$, and time τ. The NLLE differs from existing local or finite-time Lyapunov exponents defined based on linear error dynamics (Yoden and Nomura, 1993; Kazantsev, 1999; Ziehmann *et al*., 2000), which depend solely on the initial state $\mathbf{x}_0$ and time τ, not on the initial error $\boldsymbol{\delta}_0$. The ensemble mean NLLE over the global attractor of the dynamical system is given by

$$\begin{aligned}\overline{\lambda}(\boldsymbol{\delta}_0, \tau) &= \int_{\Omega} \lambda(\mathbf{x}_0, \boldsymbol{\delta}_0, \tau) d\mathbf{x} \\ &= \langle \lambda(\mathbf{x}_0, \boldsymbol{\delta}_0, \tau)\rangle_N, (N \to \infty)\end{aligned} \tag{5}$$

where Ω represents the domain of the global attractor of the system and $\langle\rangle_N$ denotes the ensemble average of samples of sufficiently large size N ($N \to \infty$). The mean relative growth of initial error (RGIE) can be obtained by

$$\overline{\Phi}(\boldsymbol{\delta}_0, \tau) = \exp[\overline{\lambda}(\boldsymbol{\delta}_0, \tau)\tau] \tag{6}$$

Using the theorem from Ding and Li (2007), we obtain

$$\overline{\Phi}(\boldsymbol{\delta}_0, \tau) \xrightarrow{P} c(N \to \infty) \tag{7}$$

where $\xrightarrow{P}$ denotes the convergence in probability and c is a constant that depends on the converged probability distribution P of error growth. The constant c can be considered as the theoretical saturation level of $\overline{\Phi}(\boldsymbol{\delta}_0, \boldsymbol{\tau})$. Once the error growth reaches the saturation level, almost all information on initial states is lost and the prediction becomes meaningless. Using the theoretical saturation level, the limit of dynamical predictability can be quantitatively determined (Li *et al*., 2006; Ding and Li, 2007; Li and Ding, 2011).

3.2. Estimating the NLLE from an observational time series

For systems whose equations of motion are explicitly known, such as the Lorenz system, we can directly calculate the mean NLLE via numerical integration of the system and its error evolution equations (Ding and Li, 2007). However, some parameters and external forcing terms in the dynamic equations of atmospheric and oceanic motion are explicitly unknown, and there exist uncertainties in determining these parameters and external forcing terms. It is possible to estimate the NLLE by making use of the large amounts of observational data available for the atmosphere and ocean. In a previous study, we developed an algorithm that yields estimates of the NLLE and its derivatives based on atmospheric observational data (Ding *et al*., 2008; Li and Ding, 2011). The general idea of the algorithm is to find local analogues of the evolution pattern from observational time series. The local analogues are searched for based on the initial information and evolution information at two different time points in the time series. If the initial distance at two different time points is small and if their evolutions are analogous over a very short interval, it is very likely that the two points were analogous at the initial time. This analogue is referred to as a 'local dynamical analogue'. A brief description of the algorithm is given in Appendix A.

As noted by Lorenz (1969), a sufficiently long time series is required when using historical analogues to study atmospheric predictability. It is almost impossible to find good natural analogues within current libraries of historical atmospheric data over large regions such as the Northern Hemisphere. However, it should be noted that the 'local dynamical analogue' is searched for from the observational time series for a small local region, for which the small number of spatial degrees of freedom makes it possible to find good local analogues within current libraries of historical atmospheric data which allows an ensemble average (Van den Dool, 1994). On the basis of atmospheric observational data, the NLLE method has been used to investigate decadal changes in weather predictability (Ding *et al*., 2008), the temporal–spatial distribution of the predictability of monthly and seasonal means of climate variables (Li and Ding, 2008), and the predictability limit of the Madden–Julian oscillation (Ding *et al*., 2010b; Ding *et al*., 2011).

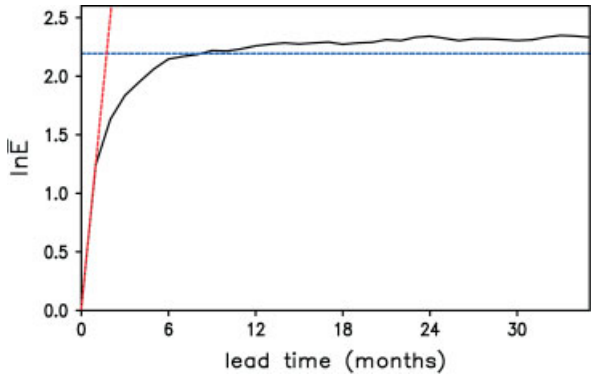

Figure 1. Time evolution of the nonlinear average growth of initial error ($\bar{E}$) for the area-averaged SST over the NINO3.4 region (solid line). The dashed red line indicates the linear average growth of initial error, as obtained by using the linear Lyapunov method (Wolf *et al*., 1985). The dashed blue line represents the 95% level of the saturation value.

To illustrate the advantage of using the NLLE method (instead of the linear Lyapunov method) to determine the predictability limit of monthly SST, we turn to the case of the area-averaged SST over the NINO3.4 region (5 °S–5 °N, 170°–120 °W). Figure 1 shows the nonlinear (as obtained by using the NLLE method) and linear (as obtained by using the linear Lyapunov method; Wolf *et al*., 1985) average growth of errors for the NINO3.4 SST. In Figure 1, there are only trivial differences between the linear and nonlinear error evolutions within a short time interval. With increasing time, however, the nonlinear error evolution begins to depart from the linear evolution and finally reaches a saturation value. In contrast, the linear error evolution shows a continuous exponential growth. To reduce the effects of sampling fluctuations, the predictability limit of SST in this study is defined as the time at which the error reaches 95% of the saturation level. From Figure 1, the predictability limit of the NINO3.4 SST, as obtained based on the nonlinear error evolution, is about 9 months, much greater than the predictability limit (only ∼2 months), as obtained based on the linear error evolution. In this study, we explore the temporal–spatial distribution of the predictability limit of reanalysis monthly SST data based on the NLLE method.

4. Annual mean predictability limit of monthly SST

Figure 2 shows the spatial distribution of the annual mean predictability limit of monthly SST. Overall, the limit of SST predictability appears to have a zonal distribution, which is more clearly seen in the zonal mean. The predictability limit in the tropical oceans is much higher than that in the extratropical oceans. In the tropical central–eastern Pacific, where ENSO events occur, the predictability limit of monthly SST exceeds 8 months. The predictability limit in the tropical Indian and Atlantic oceans is also relatively high (5–8 months). The predictability limit in the tropical Indian Ocean is generally lower than that in the tropical Pacific, possibly because the Indian Ocean climate is affected by complicated physical processes such as the strong Indian/Asian monsoon, external influences of ENSO, and chaotic intraseasonal oscillations in both the atmosphere and ocean (Luo *et al*., 2007). Variability in tropical Atlantic SST is driven by local ocean–atmosphere interaction and remote ENSO effects (Chang *et al*., 2003), resulting in lower predictability than that obtained for tropical Pacific SST. In the northern and southern mid-high latitude oceans, the ocean–atmosphere feedback is very weak and SST predictability is greatly limited by atmospheric noise; consequently, the predictability limit in these areas is small (<6 months, with a minimum value of 2–3 months). Current CGCMs show higher skill in predicting tropical SSTs than in predicting extratropical SSTs (Kug *et al*., 2007). It should be emphasized that ENSO events occur very irregularly with a timescale of 2–7 years. One year there might be no ENSO events occurring. Therefore, the predictability limit of SST in the tropical central–eastern Pacific, as calculated in the present study, does not entirely represent the predictability limit of ENSO events; it only provides a measure of the average predictability of the tropical central–eastern Pacific SST. Nevertheless,

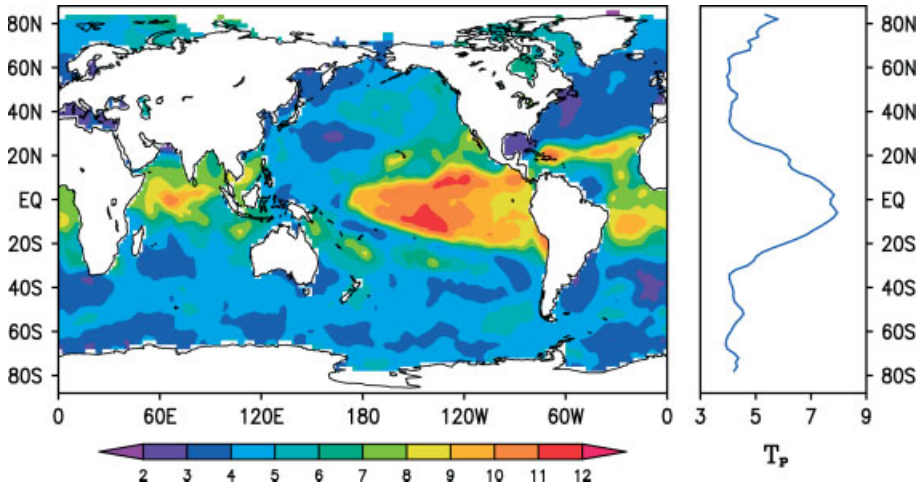

Figure 2. Spatial distribution of the annual mean predictability limit (T_p, in month) of monthly SST (left) and its zonal mean profile (right).

considering the high predictability of ENSO events, it is very likely that ENSO events make a large contribution to the predictability limit of SST in the tropical central–eastern Pacific, resulting in higher predictability in this region than in other ocean areas.

In addition to the global feature of the zonal distribution mentioned above, the limit of SST predictability shows some local characteristics. In the tropical central–eastern Pacific, the predictability limit is the highest in the NINO3.4 region (5 °S–5 °N, 170°–120 °W) (>10 months), followed by the NINO3 region (5 °S–5 °N, 150°–90 °W) and the NINO4 region (5 °S–5 °N, 160 °E–150 °W) (8–11 months), and finally the NINO1+2 region (10 °S–0°, 90°–80 °W) (~8 months). Given that predictability is the highest in the NINO3.4 region, it is most appropriate to predict NINO3.4 SST in advance using the CGCMs. The predictability limit in the tropical western Pacific is only 4–5 months, smaller than that in the tropical central–eastern Pacific. In the tropical Indian Ocean, the predictability limit is higher in the southwestern than southeastern tropical Indian Ocean. In the tropical Atlantic Ocean, the predictability limit is generally higher in the southern than northern tropical Atlantic; a region of low predictability (3–4 months) occurs off coast of the northwestern South America. In the northern mid-high latitude oceans, regions with low SST predictability are found off the east coast of continents and in the Mediterranean, where certain processes (e.g. surface runoff and human factors) affect the overall SST in a highly complex manner, resulting in lower predictability. The predictability limit in the North Pacific is around 4–6 months, greater than that in the North Atlantic (3–4 months). The distribution of the predictability limit is relatively uniform in the southern mid-high latitude oceans, consistent with the uniform terrain in the southern mid-latitudes.

5. Seasonal mean predictability limit of monthly SST

Figure 3(a)–(d) shows the spatial distribution of the predictability limit of global SST initiated from months in spring (MAM), summer (JJA), autumn (SON) and winter (DJF), respectively, revealing clear seasonal variations. Next, we separately examine variations in the seasonal mean predictability limit of SSTA in different ocean areas.

5.1. Tropical central–eastern Pacific

The limit of SST predictability in the equatorial central–eastern Pacific is very high in spring (Figure 3); large regions have a predictability limit exceeding 11 months, including both the NINO3 and NINO4 regions. The predictability limit in the NINO1+2 region is 9–10 months. In summer, the limit of SST predictability is less than that in spring, being 9–10 months in the equatorial central-eastern Pacific. Regions with a predictability limit exceeding 11 months are restricted to areas located south and north of the equatorial central–eastern Pacific. In autumn, the limit of SST predictability in the equatorial eastern Pacific shows a further decrease to 6–7 months, obviously lower than the annual mean

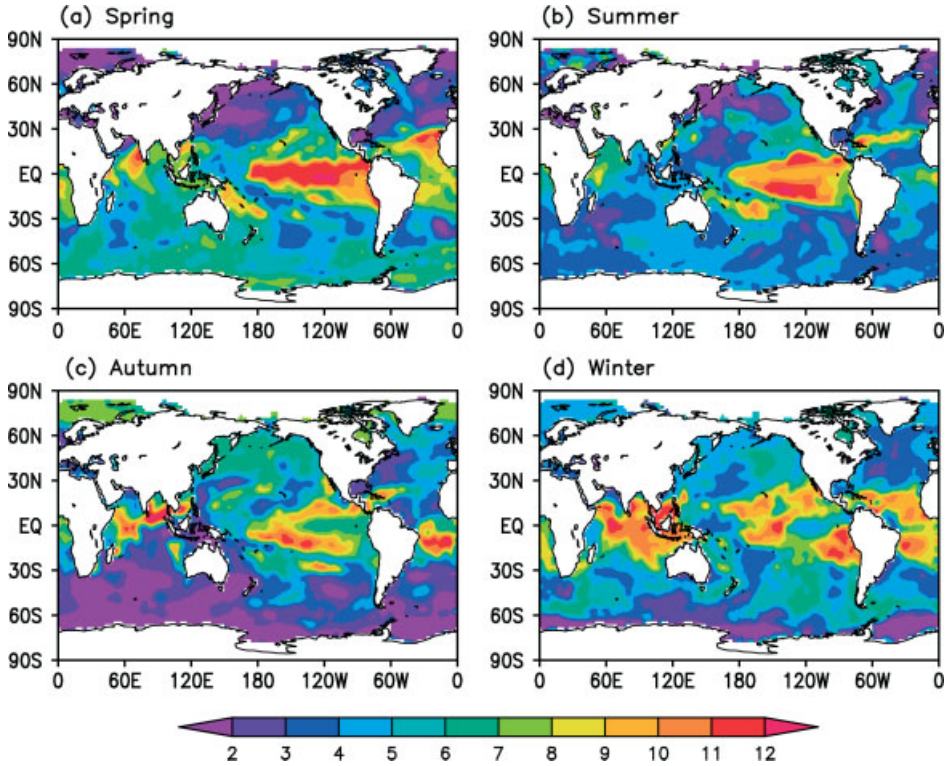

Figure 3. Spatial distribution of the predictability limit of monthly SST (in month) initiated from months in spring (MAM) (a), summer (JJA) (b), autumn (SON) (c), and winter (DJF) (d).

predictability limit. In winter, the limit of SST predictability in the equatorial eastern Pacific reaches its lowest value, being 4–5 months in the NINO3 region. Seasonal variations of SST predictability in the equatorial central–eastern Pacific can be more clearly seen from anomalies of the seasonal mean predictability limit relative to the annual mean (not shown). The predictability limit is the highest in spring, when positive anomalies occur over most of the equatorial central–eastern Pacific. The predictability limit is next highest in summer, followed by autumn and winter, when negative anomalies occur over most of the equatorial central–eastern Pacific.

Figure 4 shows seasonal variations in the area-averaged predictability limit over the NINO1+2, NINO3, NINO4, and NINO3.4 regions. Similar seasonal variations are found for the NINO3, NINO4, and NINO3.4 regions, with the highest value in spring, followed by summer and autumn, and finally winter. From spring to winter, the predictability limit shows a gradual decrease in all three of these regions, with the most pronounced decrease seen in the NINO3 region, from 11 months in spring to ~5 months in winter. As a crucial region in predicting ENSO events, the low predictability of SST in the NINO3 region makes it difficult to make long-lead predictions of ENSO events initiated from winter months. The predictability limit in the NINO1+2 region is the highest in winter, followed by spring and summer, and finally autumn, which differs from the seasonal variations in predictability limit obtained for the other three NINO regions.

In the NINO3, NINO4 and NINO3.4 regions, the low SST predictability in winter may be related to ENSO SPB. In the case that an ENSO prediction is initiated from a winter month, the forecast error would grow rapidly and reach saturation when the prediction runs across the spring, resulting in a low predictability limit in winter (Figure 5). In contrast, in the case that an ENSO prediction is initiated from a spring month, although the forecast error shows rapid initial growth, the forecast error would grow slowly in the following summer, autumn, and winter months, resulting in a relatively high predictability limit in spring. For predictions initiated from a summer month, the forecast error would grow

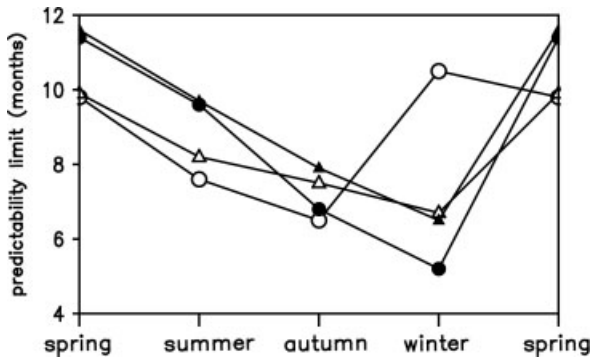

Figure 4. Seasonal variations in the predictability limit of monthly SST averaged over the NINO1+2 (open circle), NINO3 (closed circle), NINO4 (open triangle), and NINO3.4 (closed triangle) regions.

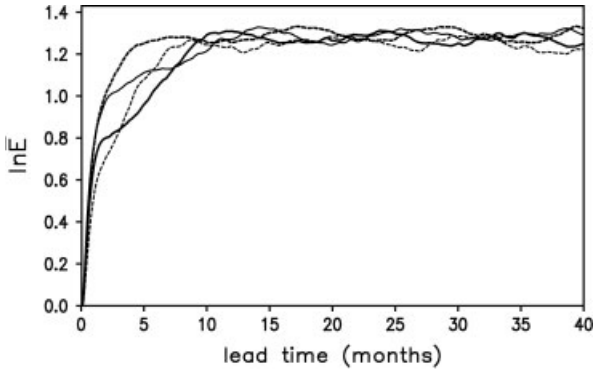

Figure 5. Time evolution of the mean relative growth of initial error ($\bar{E}$) for the NINO3 SSTA initiated from months in spring (thin solid line), summer (thick solid line), autumn (thin dashed line), and winter (thick dashed line).

slowly during the following autumn and winter months. It is only when the prediction runs across the spring of the following year that the forecast error reaches saturation and predictability is lost. Consequently, the SST predictability is higher in summer than in autumn and winter.

Saha *et al*. (2006) showed that the NCEP CFS SST retrospective forecasts experience a large drop in skill in boreal spring, but the potential predictability under perfect model assumption is less sensitive to seasons. The results of Saha *et al*. (2006) indicated that systematic model errors may be major factors limiting the predictability and degrading the forecast skill in spring. Chen *et al*. (1995) also suggested that the SPB is not intrinsic to the real climate system and that it may be a problem of the models. However, our results in the present study, as obtained from observational SST data, have indicated that ENSO SPB seems to be unrelated to the models and may be intrinsic to the real ocean–atmosphere system. The reasons for this inconsistency remain unexplained. Further study is necessary in this regard.

5.2. Tropical Indian Ocean

In the tropical Indian Ocean, the limit of SST predictability is the highest in winter, when it exceeds 8 months over most of the region (Figure 3). Especially in the southeastern tropical Indian Ocean, the predictability limit in winter is significantly higher than the annual mean predictability limit. The predictability limit is also relatively high in spring, when anomalies of the predictability limit relative to the annual mean are positive over most of the tropical Indian Ocean. The predictability limit is relatively low in summer and autumn, when it is lower than the annual mean predictability limit over most of the tropical Indian Ocean. In the southeastern tropical Indian Ocean, the predictability limit is the lowest (2–4 months) in autumn.

Saji *et al*. (1999) first introduced the Indian Ocean Dipole (IOD) to denote a basin-wide ocean–atmosphere coupled mode in the tropical Indian Ocean. The positive IOD event is characterized by positive SSTA in the

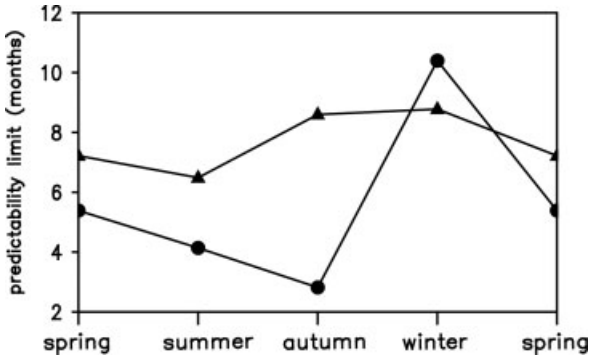

Figure 6. Seasonal variations in the predictability limit of monthly SST averaged over the southeastern tropical Indian Ocean (10 °S–0°, 90°–110 °E) (closed circle) and over the western tropical Indian Ocean (10 °S–10 °N, 50°–70 °E) (closed triangle).

western tropical Indian Ocean (10 °S–10 °N, 50°–70 °E) and negative SSTA in the southeastern tropical Indian Ocean (10 °S–0°, 90°–110 °E). Figure 6 shows seasonal variations in the area-averaged predictability limit over these two regions, revealing marked seasonal changes in the southeastern tropical Indian Ocean, where the limit is the highest in winter, followed by spring and summer, and finally autumn. The difference between the mean predictability limit for winter and autumn is as much as 7 months. In contrast, the predictability limit shows no obvious seasonal variations in the western tropical Indian Ocean, where area-averaged predictability limit is ∼8 months in all four seasons.

Similar to the phenomenon of autocorrelations of the tropical central–eastern Pacific SSTA, which show a rapid decrease in the boreal spring, Wajsowicz (2005) reported that autocorrelations of the southeastern tropical Indian Ocean SSTA show a rapid decline in the boreal winter, resulting in a winter persistence barrier (WPB). Zhao and Li (2009) also showed a similar persistence barrier of SSTA in the South China Sea and the vicinity of Indonesia around the southeastern tropical Indian Ocean. The WPB in the southeastern tropical Indian Ocean is associated with strong seasonal phase locking of the IOD. The IOD develops in summer and peaks in autumn under the positive ocean–atmosphere feedback (Saji *et al*., 1999). After reaching its peak, the IOD collapses quickly in winter due to the reversal of monsoonal winds (Li *et al*., 2003). Luo *et al*. (2007) showed that only SSTA in the southeastern tropical Indian Ocean exhibit the phenomenon of a WPB. SSTA in the western tropical Indian Ocean is more predictable in winter because of the strong influence of ENSO in this region. In the southeastern tropical Indian Ocean, the occurrence of the lowest predictability limit in autumn is probably linked to the phenomenon of WPB. The forecast error of SSTA in this region would show rapid growth when the prediction runs across winter. Given that winter follows autumn, the lowest predictability occurs in autumn. In the case that the prediction is made initiated from a winter month, although the forecast error shows rapid initial growth, the forecast error would grow slowly in the following spring, summer and autumn months; consequently, the highest predictability limit would occur in winter. As a result, influenced by the WPB, there is a large difference (as much as 7 months) in the mean predictability limit of the southeastern tropical Indian Ocean SST between winter and autumn.

Luo *et al*. (2007) showed that for the forecasts of the southeastern tropical Indian Ocean SSTA started from July, there is a robust bounce-back of the forecast skill (as measured by anomaly correlation coefficient) after winter in the SINTEX-F-coupled model. Wang *et al*. (2009) indicated that other coupled models may have similar characteristics. However, from the error growth curve of the southeastern tropical Indian Ocean SSTA (not shown), as obtained using the NLLE method, the phenomenon of the bounce-back of the forecast error is not found. This result indicates that the NLLE method has difficulty in considering the bounce-back of the forecast skill. Further work is required to extend the applicability of the NLLE method.

5.3. Tropical Atlantic

Seasonal variations in the limit of SST predictability are different in the northern tropical Atlantic (5°–20 °N, 35°–15 °W) and in the southern tropical Atlantic (20°–5 °S, 35°–10 °W) (Figure 7). The predictability limit in the northern tropical Atlantic shows similar seasonal variations to those in the southeastern tropical Indian Ocean (Figure 6), with relatively high values in winter and spring, and relatively low values in summer and autumn. In the northern tropical Atlantic, the difference in the mean predictability limit between winter and autumn exceeds 5 months. The predictability limit in the southern tropical Atlantic is the lowest in summer and the highest in winter. The predictability limit in spring and autumn is similar to that in winter. The large amplitude of seasonal variations in the predictability limit indicates that a WPB phenomenon may exist in the northern tropical Atlantic, similar to the situation in the southeastern tropical Indian Ocean. As expected, SSTA persistence in the

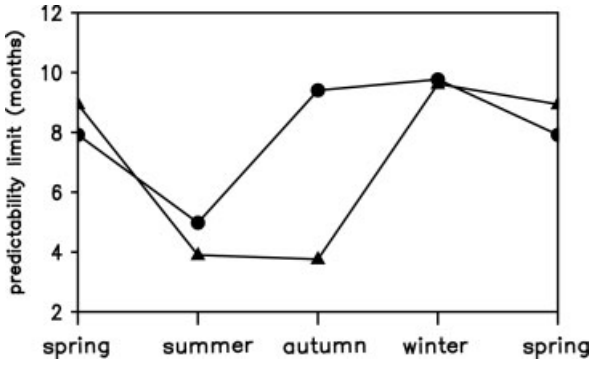

Figure 7. Seasonal variations in the predictability limit of monthly SST averaged over the southern tropical Atlantic (20°–5 °S, 35°–10 °W) (closed circle) and over the northern tropical Atlantic (5°–20 °N, 35°–15 °W) (closed triangle).

tropical northern Atlantic shows a marked decline in winter (Ding and Li, 2011). Recent studies suggest that climate variability in the tropical Atlantic sector is affected mainly by thermodynamic feedback and the remote influence of ENSO (Chang *et al*., 2003). Our results show that the WPB in the northern tropical Atlantic is due to the influence of ENSO (Ding and Li, 2011). Affected by remote ENSO forcing, the SSTA in the northern tropical Atlantic tends to be locked to the annual cycle, with ENSO peaking in winter and the SSTA in the northern tropical Atlantic peaking in the following spring. During strong El Niño events, the SSTA in the northern tropical Atlantic shows a reversal in sign and a rapid warming during winter. This sign reversal may explain the reduction in persistence, which is favorable for the occurrence of the WPB in the northern tropical Atlantic. The influence of the WPB means that the highest value of the predictability limit for the northern tropical Atlantic SST occurs in winter and the lowest value occurs in autumn.

Compared with the northern tropical Atlantic SST, the southern Atlantic tropical SST shows a weaker lead–lag correlation with the eastern tropical Pacific SST (Saravanan and Chang, 2000). Therefore, the remote effects of ENSO have a weaker influence on seasonal variations in the predictability limit of the southern tropical Atlantic SST. The low predictability of the southern tropical Atlantic SST in summer is possibly related to local physical processes in this region.

5.4. Extratropical oceans

Seasonal variations in the limit of SST predictability are similar in the North Pacific and North Atlantic (Figure 8). The predictability limit in both oceans is the highest in autumn, followed by winter and summer, and finally spring. The predictability limit in the North Pacific is much higher than that in the North Atlantic in autumn and winter, but is lower in spring and summer. Thus, the predictability limit in the North Pacific shows more pronounced seasonal fluctuations than those in the North Atlantic. In the North Pacific, the low predictability in spring and summer is possibly related to the July–September persistence barrier of SSTA (Namias and Born, 1970, 1974; Ding and Li, 2009). The seasonal differences in the persistence of North Pacific SSTA are attributed to seasonal evolutions of wind speed and its variability, which, in the North Pacific, are great in the winter months and are small in July–September. Greater wind stress is expected to result in enhanced vertical mixing in the ocean surface layers. The upper-ocean mixed layer depth in the North Pacific is observed to be the thickest in winter and the thinnest in summer. The thermal anomalies in the deep winter mixed layer are hard to change, whereas those in the shallow summer mixed layer tend to show considerable change. Therefore, the persistence of North Pacific SSTA is the weakest in July–September. The persistence of North Atlantic SSTA shows similar seasonal variations to that of North Pacific SSTA (Deser *et al*., 2003), resulting in similar seasonal variations in the predictability limit in these oceans. It remains unclear why the predictability limit in the North Pacific is much higher than that in the North Atlantic during autumn and winter. ENSO has a strong effect on the atmospheric circulation and ocean–atmosphere heat exchange over the North Pacific during winter, which in turn affects the SSTA over the North Pacific (Lau and Nath, 1996). Through this process, ENSO remote forcing is likely to contribute to the high predictability of North Pacific SSTA in autumn and winter.

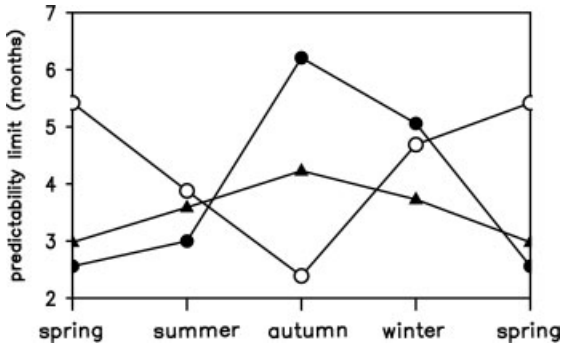

Figure 8. Seasonal variations in the predictability limit of monthly SST averaged over the North Pacific (40°–60°N, 120°E–120°W) (closed circle), over the northern Atlantic (40°–60°N, 60°W–0°) (closed triangle), and over the mid-high latitude oceans in the Southern Hemisphere (40°–60°S, 0°–360°).

In the southern mid-high latitude oceans, the predictability limit is the highest in spring and the lowest in autumn. Because the seasons are opposite in the Northern and Southern Hemispheres, seasonal variations in the predictability limit in the mid-high latitude oceans are similar in the two hemispheres. This result suggests that the same mechanisms may determine seasonal variations in the predictability limit in the mid-high latitude oceans of both hemispheres. Similar to tropical ocean SST, extratropical ocean SST also shows a seasonal persistence barrier that strongly influences seasonal variations in the predictability limit of the extratropical ocean SST. The above analysis reveals that seasonal persistence barriers exist in many oceans, and are not limited to the well-known SPB in the tropical central–eastern Pacific. Although the mechanisms that underlie the development of persistence barriers differ among the world's oceans, these barriers result in a very low limit of SST predictability when the prediction is made across the season in which the barrier occurs.

6. Summary and discussion

This study investigated that the temporal–spatial distribution of the predictability limit of monthly SST in the global oceans based on observational data. The annual mean predictability limit is very large in the tropical central–eastern Pacific (>8 months), exceeding 10 months in the NINO3.4 region; the limit is also relatively high in the tropical Indian and Atlantic oceans (5–8 months). In the northern and southern mid-high latitude oceans,

the annual mean predictability limit is relatively small (<6 months, with a minimum value of 2–3 months). The regions with the lowest SST predictability are found located off the east coast of continents in the Northern Hemisphere and in the Mediterranean.

The limit of SST predictability across most of global oceans shows significant seasonal variations. In the tropical central–eastern Pacific, the predictability limit is the highest in the boreal spring and the lowest in the boreal winter. In the NINO3, NINO4 and NINO3.4 regions, the predictability limit shows a gradual decrease from spring to winter. This reduction is most pronounced in the NINO3 region, where the predictability limit decreases from ∼11 months in spring to just 5 months in winter. The predictability limit in the southeastern tropical Indian Ocean is the highest in the boreal winter and the lowest in the boreal autumn, with a difference of 7 months between these seasons. In contrast to the southeastern tropical Indian Ocean, the predictability limit in the western tropical Indian Ocean shows no obvious seasonal variations. The predictability limit in the northern tropical Atlantic shows similar seasonal variations to those in the southeastern tropical Indian Ocean, with relatively high values in the boreal winter and spring, and relatively low values in the boreal summer and autumn. The difference of the predictability limit between winter and autumn exceeds 5 months. The predictability limit in the North Pacific and North Atlantic is the highest in the boreal autumn and the lowest in the boreal spring. Similarly, the predictability limit in the southern mid-high latitude oceans is the highest in austral autumn and the lowest in the austral spring.

The occurrence of significant seasonal variations in the predictability limit in various oceans is possibly related to the persistence barriers that occur during particular seasons. The SPB exists in the equatorial central–eastern Pacific, and the WPB exists in the southeastern tropical Indian Ocean and northern tropical Atlantic. In the North Pacific and North Atlantic, a persistence barrier of SSTA exists around July–September. These seasonal persistence barriers result in a relatively low limit of SST predictability when the prediction is made across the season in which the barrier occurs. The mechanisms responsible for the persistence barriers are different in different oceans. Because the seasonal variations in the predictability limit are obtained from observational SST data, the seasonal persistence barriers in the various oceans may be intrinsic features of the real ocean–atmosphere system. This would make it very difficult to completely eliminate the problems of the persistence barrier.

Recent studies have demonstrated that the useful forecast skill of ENSO in existing coupled models can exceed 12 months, even when initiated from months in winter (Luo *et al*., 2005, 2008; Saha *et al*., 2006). However, the predictability limit over most regions of the tropical central–eastern Pacific in winter is less than 12 months, according to our results shown in Figure 3(d). One possible reason for the relatively small predictability limit of SST in the present work is that the skill assessments of ENSO forecasts in most previous studies were based on retrospective forecasts (i.e. hindcasts). While diagnoses of the skill estimated based on hindcasts are helpful for an overall assessment of forecast systems, such estimates may not necessarily be consistent with the real-time forecast skill (Knutti, 2008; Wang *et al*., 2010). Wang *et al*. (2010) showed that beyond 2 months, the real-time forecast skill of the NINO3.4 SSTs in the NCEP Climate Forecast System (CFS) is substantially less than the 1981–2004 average hindcast skill. The predictability of ENSO estimated based on retrospective forecasts can be regarded as the potential predictability of ENSO. In contrast, the NLLE method using the reanalysis data provides an estimate of the average predictability of ENSO, which could be lower than the estimates of the potential predictability.

Another possible reason for the relatively small predictability limit of SST in the present work is that the reanalysis SST data are insufficient to find good local analogues. Li and Ding (2011) showed that if the number of experimental or observational points is insufficient to find good local analogues, the predictability limit would be underestimated. Although current libraries of historical SST data cover periods in excess of 150 years, this is likely to be insufficient to find good local analogues. Some false analogues are inevitably found in observational SST data, thereby reducing the estimated predictability limit. This may be one limitation of the NLLE method in practice if we have only a relatively short period of observational data. Since a longer period of observational SST data is unavailable, further work should employ the SST data from a long-term simulation of current coupled models (such as the 1000-year control simulation of the GFDL model), and should assess the sensitivity of the estimated SST predictability limit to the length of the period of simulation SST data. The results would be useful in understanding the extent to which the predictability limit of SST in the present work was underestimated using available reanalysis SST data.

Although the predictability limit of SST may be underestimated in the present study, the spatial variability of the predictability limit of SST could be realistic. The predictability limit of SST, as depicted in Figure 2, shows large spatial variability from the tropical to extratropical oceans, reflecting the large regional differences in local predictability limit. SST forecasts over the global oceans could benefit from an improved understanding of the spatial variability of the predictability limit of SST.

Another important point to be considered is the quality of reanalysis SST data. Considering the data requirement of the NLLE method, we investigate the temporal–spatial distributions of the limit of SST predictability in the global oceans using the ERSST data from 1854 to 2005. Due to the sparse observations before 1950 (even prior to 1973 when satellite data were not available), the ERSST data includes large uncertainty, thereby possibly introducing considerable errors in estimating the predictability limit over the global oceans (especially the extratropical oceans). Further work should be performed to compare

the results of the limit of SST predictability with other SST reanalysis or observational data.

In addition, the present study focuses on investigating the temporal–spatial distribution of the predictability limit of global SST. Little is known of the physical processes responsible for spatial differences in the SST predictability. Further study is necessary to examine the physical processes that influence local SST predictability in different oceans, as advances in this regard would result in improved forecasting models. In addition, to gain a more complete understanding of seasonal fluctuations in SST predictability, it would be necessary to investigate the mechanisms and effects of the persistence barriers.

Acknowledgements

We wish to thank the anonymous reviewers for helpful comments and suggestions, which helped to substantially improve the quality of this paper. We thank Mr. Jie Feng and Mr. Deqiang Liu for their help. This work was jointly supported by the 973 program (2010CB950400) and NSFC Projects (41175069, 41030961).

Appendix A

If we obtain the experimental data of a single variable x of an n-dimensional chaotic system, or observe the atmospheric or oceanic data of variable x at one point of n spatial grid points (e.g. the time series of x is given by $\{x(t_i), i = 0, 1, 2, \cdots\cdots, m-1\}$ where m represents the length of the time series), an algorithm that allows an estimation of the mean NLLE from the experimental or observational time series of variable x is given as follows.

Step 1. Taking $x(t_0)$ as the reference point at time t_0, we first seek the local dynamical analogue (LDA) $x(t_k)$ of the reference point from the raw series. Two distances (i.e. the initial distance between two points and the evolutionary distance between their trajectories within a short initial period) are used to measure the degree of similarity between the points. All points $x(t_j)(|t_j - t_0| > t_D$, where t_D is the time taken for autocorrelations of variable x to drop to around 0.0, ensuring that a good analogue pair is not merely due to persistence) in the raw series form a set S. The initial distance d_i between the points $x(t_0)$ and $x(t_j)$ is given by

$$d_i = |x(t_0) - x(t_j)| \tag{A1}$$

We assume that the evolutions of the two points are analogous over a very short time τ which is called the initial evolutionary interval, if they are analogous at the initial time. The choice of the initial evolutionary interval τ depends on the persistence of variable x; if the persistence is low, the time over which two initially close points remain analogous is relatively short. The time taken for autocorrelations of variable x to drop to 0.9 can be regarded as a rough estimate of the initial evolutionary interval τ. A high value (0.9) of autocorrelation is chosen to ensure a short initial evolutionary interval (the results were found to be insensitive to the selected value). Within the initial evolutionary interval τ ($\tau = K\Delta$, where Δ is the sampling interval of the time series (i.e. $\Delta = t_i - t_{i-1}$) and K is the number of sampling interval over the initial evolutionary), the evolutionary distance d_e between the two points $x(t_0)$ and $x(t_j)$ is given by

$$d_e = \sqrt{\frac{1}{K+1}\sum_{i=0}^{K}[x(t_i) - x(t_{j+i})]^2} \tag{A2}$$

d_i is the amount of the initial separation between the two points $x(t_0)$ and $x(t_j)$, while d_e is the evolutionary distance between their trajectories over the initial evolutionary. The total distance d_t, considering not only the initial distance but also the evolutionary distance, is found by adding d_i and d_e:

$$d_t = d_i + d_e \tag{A3}$$

If d_t is very small, it is highly likely that the points $x(t_0)$ and $x(t_j)$ are LDA points at the initial time. Of course, this approach is unlikely to exclude the possibility that only the variable x and its most relevant variables remain close, whereas other variables evolve very differently over time, especially for high-dimensional dynamical systems. Therefore, the analogues based on variable x are only local analogues and that they cannot simply be considered as global analogues. The constraint of the total distance d_t, which contains both initial information and evolutionary information over an initial evolutionary, allows us to exclude a large portion of all points with large initial distances, thereby helping us to find a truly local analogue of the reference point.

For every point $x(t_j)$ in the set S, the value of d_t can be determined. The nearest neighbour (LDA) $x(t_k)$ of the reference point $x(t_0)$ can be chosen from the set S only if d_t is the minimum. Then, the initial distance between $x(t_0)$ and $x(t_k)$ is denoted as follows:

$$L_1(t_0) = |x(t_0) - x(t_k)| \tag{A4}$$

Step 2. At time $\tau_i = i \times \Delta$ ($i = 1, 2, 3, \cdots\cdots, M$, where M is the total number of evolutionary steps), $x(t_0)$ will have evolved to $x(t_0 + \tau_i)$ along the reference trajectory, and $x(t_k)$ will have evolved into $x(t_k + \tau_i)$ along the analogous trajectory. The initial difference $L_1(\tau_0)$ will have become:

$$L_1(\tau_i) = |x(t_0 + \tau_i) - x(t_k + \tau_i)| \tag{A5}$$

The growth rate of the initial error during the evolutionary interval (τ_i) is

$$\xi_1(\tau_i) = \frac{1}{\tau_i}\ln\frac{L_1(\tau_i)}{L_1(0)}, (i = 1, 2, 3, \cdots\cdots, M) \tag{A6}$$

With i gradually increasing, we can obtain the variation of $\xi_1(\tau_i)$ as a function of the evolution time τ_i ($i = 1, 2, 3, \cdots\cdots, M$).

Step 3. Taking $x(t_1)$ as the reference state and evolution time $\tau_i = i \times \Delta$ ($i = 1, 2, 3, \cdots\cdots, M$), and repeating Steps 1 and 2 above, we obtain the error growth rate $\xi_2(\tau_i)$ as a function of the evolution time τ_i:

$$\xi_2(\tau_i) = \frac{1}{\tau_i} \ln \frac{L_2(\tau_i)}{L_2(0)} \tag{A7}$$

where $L_2(0)$ is the initial distance between the reference point $x(t_1)$ and its LDA, and $L_2(\tau_i)$ is the evolution of $L_2(0)$ with time τ_i.

Step 4. The above procedure is repeated until the trajectory reaches the last reference point $x(t_{m-M-1})$, we have error growth rates at all reference points $\{x(t_0), x(t_1), \cdots\cdots, x(t_{m-M-1})\}$ given by

$$\xi_k(\tau_i) = \frac{1}{\tau_i} \ln \frac{L_k(\tau_i)}{L_k(0)} \quad (k = 1, \cdots\cdots, N; i = 1, 2, 3, \cdots\cdots, M) \tag{A8}$$

where $N = m - M$ is the total number of reference points on the reference trajectory, $\tau_i = i \times \Delta$ ($i = 1, 2, 3, \cdots\cdots, M$) is the evolution time, L_k (0) is the initial distance between the reference point $x(t_k)$ and its LDA, and $L_k(\tau_i)$ is the evolution of $L_k(0)$ with the time τ_i. It follows that the average of error growth rates at all reference points is

$$\overline{\xi}(\tau_i) = \frac{1}{N} \sum_{k=1}^{N} \xi_k(\tau_i) = \frac{1}{N} \sum_{k=1}^{N} \left[\frac{1}{\tau_i} \ln \frac{L_k(\tau_i)}{L_k(0)} \right] = \frac{1}{\tau_i} \ln \left[N \sqrt{\frac{L_1(\tau_i)}{L_1(0)} \frac{L_2(\tau_i)}{L_2(0)} \cdots\cdots \frac{L_N(\tau_i)}{L_N(0)}} \right] \tag{A9}$$

That is,

$$\exp[\overline{\xi}(\tau_i)\tau_i] = N \sqrt{\frac{L_1(\tau_i)}{L_1(0)} \frac{L_2(\tau_i)}{L_2(0)} \cdots\cdots \frac{L_N(\tau_i)}{L_N(0)}} \tag{A10}$$

Step 5. Observing that the right-hand-side of Equation (A10) is the geometric mean of the relative growth of initial error (RGIE) of all reference points, we obtained the approximation of the mean RGIE:

$$\overline{\Phi}(\tau_i) = \exp[\overline{\xi}(\tau_i)\tau_i], (i = 1, 2, 3, \cdots\cdots, M) \tag{A11}$$

By investigating the evolution of $\overline{\Phi}(t_i)$ with increasing τ_i, we can estimate the mean predictability limit of the variable x.

References

Astudillo HF, Borotto FA, Abarca-del-Rio R. 2010. Embedding reconstruction methodology for short time series-application to large El Niño events. *Nonlinear Processes in Geophysics* **17**: 753–764.

Barnston AG, Glanz MH, He Y. 1999. Predictive skill of statistical and dynamical climate models in forecasts of SST during the 1997–98 El Niño episode and the 1998 La Niña onset. *Bulletin of the American Meteorological Society* **80**: 217–243.

Bengtsson L, Schlese U, Roeckner E, Latif M, Barnett TP, Graham NE. 1993. A two-tiered approach to long-range climate forecasting. *Science* **261**: 1027–1029.

Chang P, Saravanan R, Ji L. 2003. Tropical Atlantic seasonal predictability: the roles of El Niño remote influence and thermodynamic air-sea feedback. *Geophysical Research Letters* **30**: 1501, DOI: 10.1029/2002GL016119.

Chen BH, Li JP, Ding RQ. 2006. Nonlinear local Lyapunov exponent and atmospheric predictability research. *Science in China* **49**: 1111–1120.

Chen DK, Zebiak SE, Busalacchi AJ, Cane MA. 1995. An improved procedure for El Niño forecasting: implications for predictability. *Science* **269**: 1699–1102.

Chowdary JS, Xie SP, Lee JY, Kosaka Y, Wang B. 2010. Predictability of summer Northwest Pacific climate in eleven coupled model hindcasts: local and remote forcing. *Journal of Geophysical Research* **115**: D22121, DOI: 10.1029/2010JD014595.

Chowdary JS, Xie SP, Luo JJ, Hafner J, Behera S, Masumoto Y, Yamagata T. 2011. Predictability of Northwest Pacific climate during summer and the role of the tropical Indian Ocean. *Climate Dynamics* **36**: 607–621.

Collins M, Frame D, Sinha B, Wilson C. 2002. How far ahead could we predict El Niño? *Geophysical Research Letters* **29**: 1492, DOI: 10.1029/2001GL013919.

Davis R. 1978. Predictability of sea level pressure anomalies over the North Pacific Ocean. *Journal of Physical Oceanography* **8**: 233–246.

Deser C, Alexander MA, Timlin MS. 2003. Understanding the persistence of sea surface temperature anomalies in midlatitudes. *Journal of Climate* **16**: 57–72.

Ding RQ, Li JP. 2007. Nonlinear finite-time Lyapunov exponent and predictability. *Physics Letters A* **364**: 396–400.

Ding RQ, Li JP. 2009. Decadal and seasonal dependence of North Pacific SST persistence. *Journal of Geophysical Research* **114**: D01105, DOI: 10.1029/2008JD010723.

Ding RQ, Li JP. 2011. Winter persistence barrier of sea surface temperature in the northern tropical Atlantic associated with ENSO. *Journal of Climate* **24**: 2285–2299.

Ding RQ, Li JP, Ha KJ. 2008. Trends and interdecadal changes of weather predictability during 1950s-1990s. *Journal of Geophysical Research* **113**: D24112, DOI: 10.1029/2008JD010404.

Ding RQ, Ha KJ, Li JP. 2010a. Interdecadal shift in the relationship between the East Asian summer monsoon and the tropical Indian Ocean. *Climate Dynamics* **34**: 1059–1071.

Ding RQ, Li JP, Seo KH. 2010b. Predictability of the Madden–Julian oscillation estimated using observational data. *Monthly Weather Review* **138**: 1004–1013.

Ding RQ, Li JP, Seo KH. 2011. Estimate of the predictability of boreal summer and winter intraseasonal oscillations from observations. *Monthly Weather Review* **139**: 2421–2438.

Eckmann JP, Ruelle D. 1985. Ergodic theory of chaos and strange attractors. *Reviews of Modern Physics* **57**: 617–656.

Folland CK, Palmer TN, Parker DE. 1986. Sahel rainfall and worldwide sea temperatures, 1901–85. *Nature* **320**: 602–607.

Frankignoul C, Sennéchael N. 2007. Observed influence of North Pacific SST anomalies on the atmospheric circulation. *Journal of Climate* **20**: 592–606.

Frederiksen CS, Zhang HQ, Balgovind RC, Nicholls N, Drosdowsky W, Chambers L. 2001. Dynamical seasonal forecasts during the 1997/98 ENSO using persisted SST anomalies. *Journal of Climate* **14**: 2675–2695.

Goswami BN, Shukla J. 1991. Predictability of the coupled ocean-atmosphere model. *Journal of Climate* **4**: 3–22.

Guan Z, Yamagata T. 2003. The unusual summer of 1994 in East Asia: IOD teleconnections. *Geophysical Research Letters* **30**: 1544–1547.

Jin EK, Kinter JL, Wang B, Park CK, Kang IS, Kirtman BP, Kug JS, Kumar A, Luo JJ, Schemm J, Shukla J, Yamagata T. 2008. Current status of ENSO prediction skill in coupled ocean-atmosphere models. *Climate Dynamics* **31**: 647–664.

Kang IS, Shukla J. 2006. Dynamic seasonal prediction and predictability of the monsoon. In *The Asian Monsoon*, Wang B (ed). Springer-Praxis: Chichester, 585–612.

Kazantsev E. 1999. Local Lyapunov exponents of the quasi–geostrophic ocean dynamics. *Applied Mathematics and Computation* **104**: 217–257.

Knutti R. 2008. Should we believe model predictions of future climate change? *Philosophical Transactions of the Royal Society A* **366**: 4647–4664.

Kug JS, Lee JY, Kang IS. 2007. Global sea surface temperature prediction using a multimodel ensemble. *Monthly Weather Review* **135**: 3239–3247.

Lacarra JF, Talagrand O. 1988. Short-range evolution of small perturbations in a baratropic model. *Tellus* **40A**: 81–95.

Latif M, Anderson D, Barnett T, Cane M, Kleeman R, Leetmaa A, O'Brien J, Rosati A, Schneider E. 1998. A review of the predictability and prediction of ENSO. *Journal of Geophysical Research* **103**: 14375–14394.

Lau NC, Nath MJ. 1996. The role of the atmospheric bridge in linking tropical Pacific ENSO events to extratropical SST anomalies. *Journal of Climate* **9**: 2036–2057.

Lau KM, Weng HY. 1999. Interannual, decadal-interdecadal, and global warming signals in sea surface temperature during 1955–97. *Journal of Climate* **12**: 1257–1267.

Li JP, Ding RQ. 2008. Temporal-spatial distributions of predictability limit of short-term climate (in Chinese with English abstract). *Chinese Journal of Atmospheric Sciences* **32**: 975–986.

Li JP, Wang S. 2008. Some mathematical and numerical issues in geophysical fluid dynamics and climate dynamics. *Communications in Computational Physics* **3**: 759–793.

Li JP, Ding RQ. 2011. Temporal–spatial distribution of atmospheric predictability limit by local dynamical analogues. *Monthly Weather Review* **139**: 3265–3283.

Li T, Wang B, Chang CP, Zhang Y. 2003. A theory for the Indian Ocean dipole-zonal mode. *Journal of Atmospheric Sciences* **60**: 2119–2135.

Li JP, Ding RQ, Chen BH. 2006. Review and prospect on the predictability study of the atmosphere. In *Review and Prospects of the Developments of Atmosphere Sciences in Early 21st Century*, National Nature Science Foundation of China (NSFC), (eds) China Meteorology Press: Beijing, 96–104.

Li JP, Wu ZW, Jiang ZH, He JH. 2010. Can global warming strengthen the East Asian summer monsoon? *Journal of Climate* **23**: 6696–6705.

Li JP, Feng J, Li Y. 2011. A possible cause of decreasing summer rainfall in northeast Australia. *International Journal of Climatology* **32**: 995–1005.

Lorenz EN. 1965. A study of the predictability of a 28-variable atmospheric model. *Tellus* **17**: 321–333.

Lorenz EN. 1969. Atmospheric predictability as revealed by naturally occurring analogues. *Journal of Atmospheric Sciences* **26**: 636–646.

Luo JJ, Masson S, Behera S, Shingu S, Yamagata T. 2005. Seasonal climate predictability in a coupled OAGCM using a different approach for ensemble forecast. *Journal of Climate* **18**: 4474–4497.

Luo JJ, Masson S, Behera S, Yamagata T. 2007. Experimental forecasts of Indian Ocean dipole using a coupled OAGCM. *Journal of Climate* **20**: 2178–2190.

Luo JJ, Masson S, Behera S, Yamagata T. 2008. Extended ENSO predictions using a fully coupled ocean-atmosphere model. *Journal of Climate* **21**: 84–93.

Mu M. 2000. Nonlinear singular vectors and nonlinear singular values. *Science in China (D)* **43**: 375–385.

Namias J. 1986. Persistence of flow patterns over North America and adjacent ocean section. *Monthly Weather Review* **114**: 1368–1383.

Namias J, Born RM. 1970. Temporal coherence in North Pacific sea surface temperature patterns. *Journal of Geophysical Research* **75**: 5952–5955.

Namias J, Born RM. 1974. Further studies of temporal coherence in North Pacific sea surface temperature patterns. *Journal of Geophysical Research* **79**: 797–798.

Nnamchi HC, Li JP. 2011. Influence of the South Atlantic ocean dipole on West African summer precipitation. *Journal of Climate* **24**: 1184–1197.

Nnamchi HC, Li JP, Anyadike R. 2011. Does a dipole mode really exist in the South Atlantic Ocean? *Journal of Geophysical Research* **116**: D15104, DOI: 10.1029/2010JD015579.

Palmer TN, Anderson DLT. 1994. The prospects for seasonal forecasting – a review paper. *Bulletin of the American Meteorological Society* **120**: 755–793.

Peng P, Kumar A, Barnston AG, Goddard L. 2000. Simulation skills of the SST-forced global climate variability of the NCEP-MRF9 and the Scripps-MPI ECHAM3 models. *Journal of Climate* **13**: 3657–3679.

Philander SGH. 1990. *El Niño, La Niña and the Southern Oscillation*. Academic Press: San Diego, 289. pp.

Repelli CA, Nobre P. 2004. Statistical prediction of sea-surface temperature over the tropical Atlantic. *International Journal of Climatology* **24**: 45–55.

Rogberg P, Read PL, Lewisb SR, Montaboneb L. 2010. Assessing atmospheric predictability on Mars using numerical weather prediction and data assimilation. *Quarterly Journal of the Royal Meteorological Society* **136**: 1614–1635.

Saha S, Nadiga S, Thiaw C, Wang J, Wang W, Zhang Q, Van den Dool HM, Pan HL, Moorthi S, Behringer D, Stokes D, Peña M, Lord S, White G, Ebisuzaki W, Peng P, Xie P. 2006. The NCEP climate forecast system. *Journal of Climate* **19**: 3483–3517.

Saji NH, Goswami BN, Vinayachandran PN, Yamagata T. 1999. A dipole mode in the tropical Indian Ocean. *Nature* **401**: 360–363.

Saravanan R, Chang P. 2000. Interaction between tropical Atlantic variability and El Niño-Southern Oscillation. *Journal of Climate* **13**: 2177–2194.

Smith TM, Reynolds RW. 2004. Improved extended reconstruction of SST (1854–1997). *Journal of Climate* **17**: 2466–2477.

Stockdale TN, Balmaseda MA, Vidard A. 2006. Tropical Atlantic SST prediction with coupled ocean-atmosphere GCMs. *Journal of Climate* **19**: 6047–6061.

Stockdale TN, Anderson DLT, Balmaseda MA, Doblas-Reyes F, Ferranti L, Mogensen K, Palmer TN, Molteni F, Vitart F. 2011. ECMWF seasonal forecast system 3 and its prediction of sea surface temperature. *Climate Dynamics* **37**: 455–471.

Taschetto AS, Wainer I. 2008. The impact of the subtropical South Atlantic SST on South American precipitation. *Annales Geophysicae* **26**: 3457–3476.

Trenberth KE, Branstator GW, Karoly D, Kumar A, Lau NC, Ropelewski C. 1998. Progress during TOGA in understanding and modeling global teleconnections associated with tropical sea surface temperatures. *Journal of Geophysical Research* **103**: 14291–14324.

Van den Dool HM. 1994. Searching for analogues, how long must we wait? *Tellus* **46A**: 314–324.

Wajsowicz RC. 2005. Potential predictability of tropical Indian Ocean SST anomalies. *Geophysical Research Letters* **32**: L24702, DOI: 10.1029/2005GL024169.

Wang B, Lee JY, Shukla J, Kang IS, Shukla J, Park CK, Kumar A, Schemm J, Cocke S, Kug JS, Luo JJ, Zhou T, Wang B, Fu X, Yun WT, Alves O, Jin EK, Kinter J, Kirtman Krishnamurti T, Lau NC, Lau W, Liu P, Pegion P, Rosati T, Schubert S, Stern W, Suarez M, Yamagata T. 2009. Advance and prospectus of seasonal prediction: Assessment of APCC/CliPAS 14-model ensemble retrospective seasonal prediction (1980–2004). *Climate Dynamics* **33**: 93–117.

Wang WQ, Chen MY, Kumar A. 2010. An assessment of the CFS real-time seasonal forecasts. *Weather and Forcasting* **25**: 950–969.

Webster PJ, Yang S. 1992. Monsoon and ENSO: selectively interactive systems. *Quarterly Journal of the Royal Meteorological Society* **118**: 877–925.

Wolf A, Swift JB, Swinney HL, Vastano JA. 1985. Determining Lyapunov exponents from a time series. *Physica D* **16**: 285–317.

Wu LX, Liu ZY. 2004. Atmospheric response to North Pacific SST: The role of Ocean-Atmosphere coupling. *Journal of Climate* **17**: 1859–1882.

Wu ZW, Wang B, Li JP, Jin FF. 2009. An empirical seasonal prediction model of the East Asian summer monsoon using ENSO and NAO. *Journal of Geophysical Research* **114**: D18120, DOI: 10.1029/2009JD011733.

Wu ZW, Li JP, Jiang ZH, He JH, Zhu XY. 2011. Possible effects of the North Atlantic Oscillation on the strengthening relationship between the East Asian summer monsoon and ENSO. *International Journal of Climatology* **32**: 794–800, DOI: 10.1002/JOC.2309.

Yoden S, Nomura M. 1993. Finite-time Lyapunov stability analysis and its application to atmospheric predictability. *Journal of Atmospheric Sciences* **50**: 1531–1543.

Zhao X, Li JP. 2009. Possible causes for the persistence barrier of SSTA in the South China Sea and the vicinity of Indonesia. *Advances in Atmospheric Sciences* **26**: 1125–1136.

Zhao X, Li JP. 2010. Winter-to-winter recurrence of sea surface temperature anomalies in the Northern Hemisphere. *Journal of Climate* **23**: 3835–3854.

Ziehmann C, Smith LA, Kurths J. 2000. Localized Lyapunov exponents and the prediction of predictability. *Physics Letters A* **4**: 237–251.

